Journal of Physics D: Applied Physics

**PAPER** • **OPEN ACCESS**

# A study of the formation of fuzzy tungsten in a HiPIMS plasma system

To cite this article: Zeyad Ali *et al* 2024 *J. Phys. D: Appl. Phys.* **57** 175202

OPEN ACCESS
IOP Publishing
Journal of Physics D: Applied Physics
J. Phys. D: Appl. Phys. **57** (2024) 175202 (9pp)
https://doi.org/10.1088/1361-6463/ad2005

# A study of the formation of fuzzy tungsten in a HiPIMS plasma system

**Zeyad Ali**[1], **Mounib Bahri**[2], **Matthew Bilton**[2] and **James W Bradley**[1,*]

[1] Department of Electrical Engineering and Electronics, University of Liverpool, Brownlow Hill, Liverpool L69 3GJ, United Kingdom
[2] Albert Crewe Centre for Electron Microscopy, University of Liverpool, Liverpool, Brownlow Hill, Liverpool L69 3GL, United Kingdom

E-mail: jbradley@liverpool.ac.uk

Received 21 September 2023, revised 22 December 2023
Accepted for publication 18 January 2024
Published 1 February 2024

**Abstract**

Nanostructured 'fuzzy' tungsten has been grown for the first time in a high-power impulse magnetron sputtering high power-impulse magnetron sputtering-(HiPIMS) system. The fuzzy layers were formed over range of surface temperatures $T_{s,}$ from 1025 to 1150 K, for helium ion fluences of $5.02 \times 10^{24}$ m$^{-2}$, and mean ion bombardment energy of 55 eV. The time-evolution of the helium ion flux ($\Gamma_{He}$) and incident energy ($E_{He}$) were determined during the HiPIMS pulse (of width of 150 $\mu$s) using a planar Langmuir probe. The micrographic findings revealed that, the thickness of HiPIMS-grown nano-tendrill layers increased by 83% (from 274 to 501 nm) for only a 125 K rise in $T_s$. This result is explained by the fact that higher surface temperatures led to larger helium bubbles which ultimately produce a thicker nanostructured layer. The growth rate of fuzzy tungsten layers in HiPIMS conditions is approximately 50% lower than those observed for DC magnetron operation.

Keywords: nanotendril, fuzz, nanostructured, tungsten, helium, HiPIMS, Langmuir probe

## 1. Introduction

Tungsten has been chosen as a plasma-facing material for the international-thermonuclear Experimental Reactor (ITER) due to its extremely high melting point, limited retention of hydrogen isotopes, relatively high thermal conductivity and low sputtering rate [1–4]. However, there is a challenge posed by the fact that helium (He) plasma irradiation may affect the morphology of a tungsten surface. Particularly, when a pure tungsten surface in the temperature range ($1000 < T_s < 2000$ K), is exposed to a high fluence ($\Phi_{He} > 1 \times 10^{24}$ m$^{-2}$) of energetic helium ions (energies $E_{He} > 25$ eV), nanotendril surface structure known as 'fuzz' can form [5, 6]. Experimental studies have shown that the thickness of fuzzy tungsten ranges from a few hundred nanometers up to mm's [7] with the porosities of nanotendrils tungsten in excess of 90% [8]. Additionally, the optical reflectivity of a fuzzy layer can rather low for instance around 1% [9]. Baldwin and Doerner [8] showed that the thickness of the fuzzy tungsten (W) layer increases with the square root of the plasma irradiation time (Fick's law). The presence of nanostructures tungsten in tokamaks, such as Alcator C-Mo, COMPASS, and WEST divertors, raises questions about the lifespan of components in fusion nuclear power stations [10–12].

Linear plasma devices (LPD's) have been employed for the majority of fuzzy-tungsten studies due to the production of a high helium (He) ion flux ($\Gamma_{He} > 1 \times 10^{21}$ m$^{-2}$ s) to an electrically biased W sample. Consequently, plasma-exposed samples obtain sufficient temperature for the fuzz growth process without using an external heating system [13–15]. Recently, an alternative technique has been demonstrated to investigate fuzzy-tungsten by utilizing a magnetron

* Author to whom any correspondence should be addressed.

sputtering discharge [16, 17]. In these systems, the bombarding ion fluences are somewhat lower than in LPD's with $\Gamma_{He} \sim 10^{20}$ $m^{-2}s$, with typically tungsten surface temperature from 900–1200 K, and ion-bombarding energy from 25–100 eV. In the magnetron technique, elevated heating caused by energetic ions is avoided, allowing the samples temperature to be controlled using an additional heating source. Petty and Bradley [18] demonstrated the growth of fuzzy tungsten in a DC magnetron sputtering (DCMS) system, fitted with a tungsten target, operating in helium gas. One major difference between the LPD and magnetron-gown fuzzy layers is that in the latter there is an intrinsic auxiliary source of tungsten W from the magnetron cathode target (also fixed to be W) due to low but detectable rates of helium ion sputtering. It has been shown in a number of studies that fuzzy tungsten growth rates (and the ultimate layer thicknesses) can be increased significantly if the heated W sample is being deposited upon from an auxiliary source of tungsten [7, 17, 19, 20].

Here, we use a high power-impulse magnetron sputtering-(HiPIMS) to form fuzzy tungsten layers. HiPIMS is a relatively new (PVD) technique developed for the deposition of engineering quality thin films due to an intrinsic capacity to produce a high-density plasma ($10^{18}$–$10^{19}$ $m^{-3}$) with a highly ionized-metal fractions ($\geqslant$70%). HiPIMS- discharges are powered by applying a negative-short pulse (20–500 $\mu$s) with a power density (0.5–10 kW $cm^{-2}$) at a magnetron target. In this technique, a low-duty cycle used to prevent a target material from melting [21]. With the use sample- biasing HiPIMS provides a tool to deposit thin films using predominately plasma ions rather than neutral sputtered particles (as in DC sputtering) with controlled and defined energy leading to a significant enhancement in the structural characteristics of a grown thin-film. HiPIMS also offers the possibility with certain metals to attain self-sputtering [22]. As a consequence, HiPIMS technique produces harder, smoother, and denser—thin films than the films generated by mean of DC- conventual magnetron sputtering method [23]. However, the growth and deposition rates $R$ obtained from HiPIMS plasma are often smaller than the in DC or pulsed DC magnetron-sputtering (for the same average-input power) due to the strong back attraction of metal ions the cathode target [22].

In this study, we used a HiPIMS system operating in helium gas for the first time to grow a fuzzy layer on a bulk tungsten sample. The experiment was carried out with a fixed average helium ion fluence, incident energy, and surface temperature range (1025–1150 K). The nanostructured tungsten grown using HiPIMS was compared with the layer produced in DC sputtering conditions at the same temperature range. As described further below our results are consistent with recent studies, indicating that the growth of nano-tendrils is likely influenced by the deposition of W atoms onto the fuzzy layer during plasma irradiation.

## 2. Experimental setup

The magnetron-sputtering system consists of an unbalanced circular magnetron (V150-TechTM) housed in a 40 cm inner diameter $\times$ 70 cm length stainless steel vessel (provided by Gencoa Ltd). The system is fitted with a 6-inch tungsten target (99.95% purity). The vacuum chamber was evacuated to a base pressure of $3 \times 10^{-6}$ torr using a Leybold-NT 1000 $Ls^{-1}$ turbo-molecular pump backed by an Edwards-E2M40 rotary pump.

Helium gas (of 99.995% purity) was admitted into the vessel using a mass flow controller (type MKS Instruments-250) and the chosen operating pressure of 6 Pa during the fuzz growth process was monitored by a Baratron gauge (MKS Instruments-627). The magnetron system was driven by a HiPIMS unit (Impulse 2–2, a Starfire Industries) supported by a DC power supply (Kurt J. Lesker, PD500X3) as illustrated in figure 1.

The discharge current and voltage were displayed on an oscilloscope (type Textronix TDS3014). The average HiPIMS-plasma power, the negative-pulse width and a repetition frequency were fixed at 800 W, 150 $\mu$s and 1.2 kHz respectively.

A tungsten circular disc (of 99.95% purity) of 1 cm diameter and 0.5 mm thickness (manufactured by Goodfellow Ltd) was vertically mounted, 60 mm away and facing the magnetic trap (racetrack) of the tungsten magnetron target surface. This acted as the substrate from which the fuzzy surface grow. Prior to mounting in the system, the tungsten samples were mechanically polished using P600 dry/wet sandpaper, followed by KOH electro-polishing to mirror-finish, and then immersed in a propanol-ultrasonic bath for ten minutes to eliminate any tiny particles. The tungsten sample was biased at a potential of $V_b = -55$ volts using a DC power supply to provide a helium ion bombarding energy of 54 eV ($E_{He} = V_p - V_b$), where $V_p$ is the local plasma potential measured at $-1$ V.

The tungsten sample substrates were heated (by direct resistance heating) through the application of a low voltage (typically 2 V) across them. The samples were fitted to two vertical copper rods via two small tungsten springs, this provided high heating current (up to $I \sim 40$ A), see figure 1. This approach to sample heating is different from electron bombardment heating as used in previous studied in the system [18]. The tungsten surface temperature was measured using a type K- thermocouple situated behind it and a Micro-Epsilon IR pyrometer (with a wavelength of 2.3 $\mu$m), which viewed the sample (typically with surface emissivity of 0.33) via a vacuum window from outside the vacuum vessel. Furthermore, $T_s$ remains approximately constant throughout a HiPIMS pulse because the power delivered to the tungsten (W) sample from the plasma is significantly smaller than the resistive heating power.

Figure 2(a) shows a plot of the discharge current and voltage traces during the negative pulse and near afterglow phases of the HiPIMS pulse cycle. The time-resolved I–V Langmuir probe characteristics (as illustrated in figure 2(b)) were carried out using a computerized acquisition system (type ALP, 150 Impedans Ltd), supported by an internal delay generator with a time resolution of 12.5 ns. This ensured synchronization with the pulse generator within the Starfire HiPIMS unit. The acquisition time ranged from 0 to 840 $\mu$s in steps of 10 $\mu$s. The sweeping voltage of the planner Langmuir

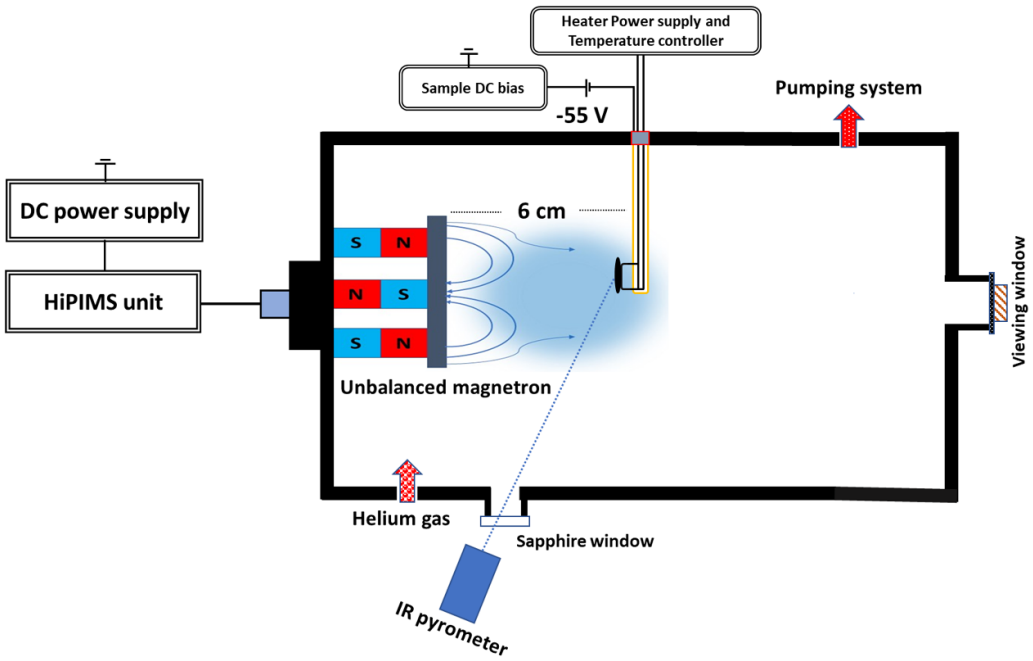


**Figure 1.** A schematic diagram of the HiPIMS discharge setup, including the vertically mounted W sample and resistance heater system.

probe for each 10 $\mu$s interval was varied in increments of 0.1 V, ranging from −100 V to 20 V. The probe tip had the same diameter as a disk tungsten sample (10 mm). At an average discharge power of 800 W and helium pressure of 6 Pa, over the entire pulse period ($T = 833$ $\mu$s), the average bombarding ion flux density and energy were $(2.325 \pm 0.06) \times 10^{20} \mathrm{m}^{-2}\,\mathrm{s}^{-1}$ and 54.9 eV respectively, calculated from data in figures 2 (c) and (d).

Focused ion beam (FIB-SEM) microscope (type FEI Helios Nanolab 600i) was utilized to conduct a surface analysis. Surface cross-sections were milled using a gallium ion beam, which were then measured and imaged to determine the thickness of the fuzz layer. Protective layers made of platinum and carbon has been first deposited on the nanostructured surface before milling out length cross-sections of around 25 $\mu$m. In order to obtain detailed and high-resolution images on the fuzzy tungsten, scanning transmission electron microscopy (STEM) analysis was carried out by preparing samples using FIB milling and examining them using scanning-transmission electron microscope (type a JEOL 2100F FEG). Both HAADF-high angle annular dark-field STEM and bright-field (BF) STEM imaging techniques were employed to capture images of the fuzzy tungsten. Bruker Nanoscope atomic force microscopy was used to measure the tungsten surface roughness.

## 3. Results and discussion

Six tungsten samples were exposed to helium plasma created in DCMS and HiPIMS discharge conditions respectively. To provide a comprehensive overview, table 1 summarizes the plasma exposure parameters and corresponding measurements of the nanostructured tungsten thickness. After six hours of HiPIMS discharge treatment, the tungsten sample turned optically black.

### *3.1. The effect of a surface temperature on fuzzy W grown in DC magnetron conditions*

Figures 3(a)–(f) shows SEM-FIB and cross-sectional micrographs of three tungsten surfaces irradiated by DC Helium plasma at surface temperatures ranging from 1125 to 1150 K, with a He ion fluence of $6.54 \times 10^{24}$ m$^{-2}$ (of 18 h plasma treatment) and an ion bombarding energy of 54 eV. These surface temperatures were chosen based on the temperature range of the ITER divertor (300–1200 K) and are within the fuzz temperature window (900–1900 K) [6]. With an increase in surface temperature from 1025 to 1150 K, we see an increase the thickness of a fuzzy layer grown from $1398 \pm 63$–$2858 \pm 32$ nm. This trend is consistent with previous studies in the magnetron system [16, 17]. This finding suggests a possible correlation between the formation of nanostructured tungsten and helium bubbles when the tungsten surface temperature exceeded 1000 K. The vacancy formation's activity is a crucial factor that significantly influences the formation and expansion of nano-bubbles, thereby contributing to the enhanced growth rate of the fuzzy layer [24].

Since the morphology and growth characteristics are well documented for fuzzy surfaces grown in DC magnetron conditions we herein concentration on new results for HiPIMS operation.

### *3.2. The effect of a surface temperature on HiPIMS-grown fuzzy W*

To investigate the effect of surface temperatures (1025–1150 K) on the nano-tendril width and the thickness

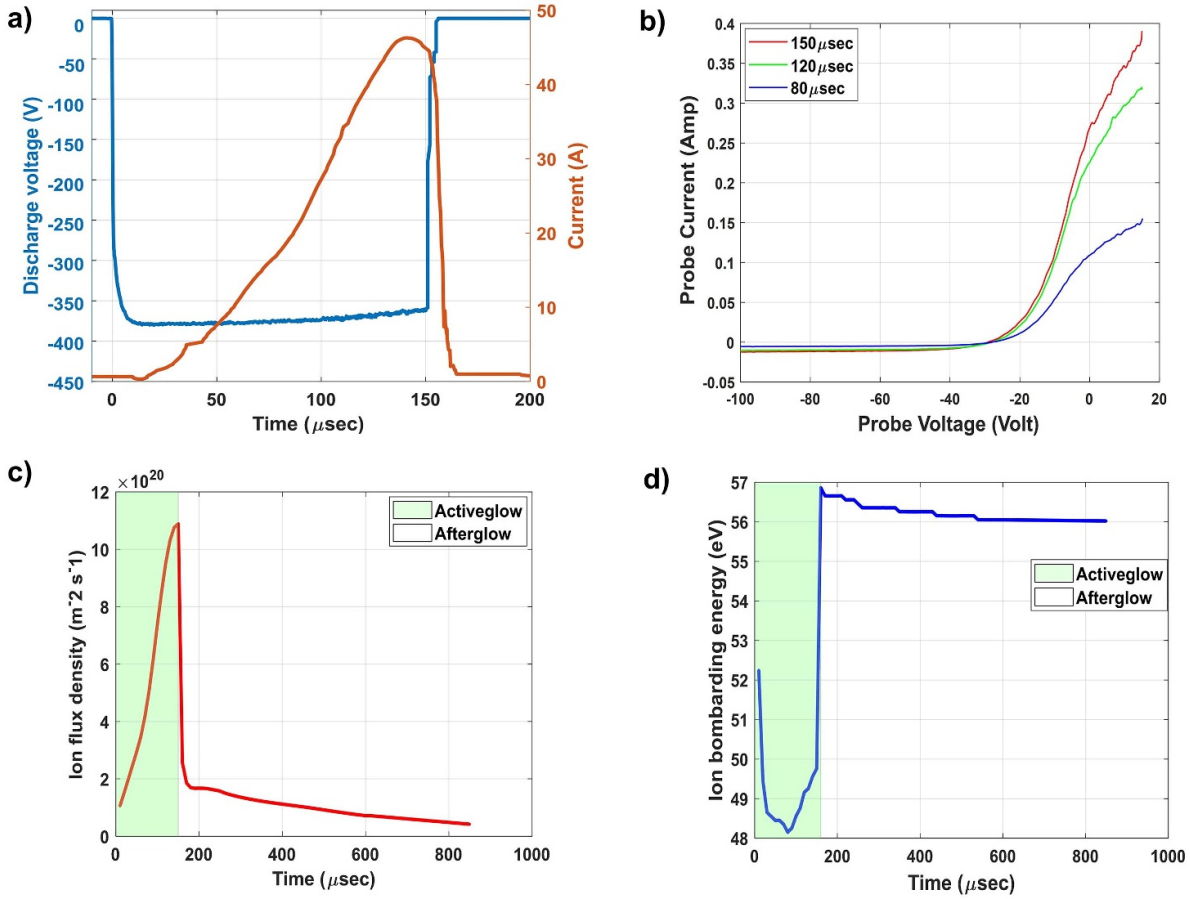


**Figure 2.** Plots of (a) the discharge current-voltage waveforms during the HiPIMS pulse cycle, (b) Time-resolved Langmuir probe I–V characteristics obtained from a HiPIMS discharge for three acquisition times, (c) the time-evolution of bombarding helium ion flux density and (d) the ion bombarding energy as determined from the Langmuir probe measurements.

**Table 1.** The tungsten sample exposure conditions and the thickness of all fuzzy layers obtained from this study. Sample temperature $T_s$, bombarding energy $E_{He}$, bombarding ion flux density $\Gamma_{He}$, exposure time $T$, ion fluence $\Phi_H$, fuzzy layer thickness $h_{fuzz}$, and mean fuzzy layer growth rate $dh_{fuzz}/dt$.

| Plasma | $T_s$ ±40 K | $E_{He}$ (eV) | $\Gamma_{He}$ ($m^{-2}$ $s^{-1}$)×$10^{20}$ | $T(h)$ | $\Phi_{He}$ $(m^{-2})$ × $10^{24}$ | $h_{fuzz}$ (nm) | $dh_{fuzz}/dt$ (nm $min^{-1}$) |
|---|---|---|---|---|---|---|---|
| DCMS | 1025 | 54 | 1.01 ± 0.04 | 18 | 6.54 ± 0.26 | 1398 ± 63 | 1.294 ± 0.06 |
| DCMS | 1100 | 54 | 1.01 ± 0.04 | 18 | 6.54 ± 0.26 | 1701 ± 30 | 1.575 ± 0.03 |
| DCMS | 1150 | 54 | 1.01 ± 0.04 | 18 | 6.54 ± 0.26 | 2858 ± 32 | 2.646 ± 0.03 |
| HiPIMS | 1025 | 54.91 | 2.325 ± 0.06 | 6 | 5.02 ± 0.12 | 274.5 ± 10 | 0.762 ± 0.03 |
| HiPIMS | 1100 | 54.91 | 2.325 ± 0.06 | 6 | 5.02 ± 0.12 | 378 ± 10 | 1.05 ± 0.03 |
| HiPIMS | 1150 | 54.91 | 2.325 ± 0.06 | 6 | 5.02 ± 0.12 | 501 ± 12 | 1.391 ± 0.03 |

of the fuzz layer grown in a helium HiPIMS discharge, tungsten (W) samples were irradiated for with ion fluence of $5.02 \times 10^{24}$ $m^{-2}$ (of 6 h plasma treatment) and time-averaged ion bombarding energy of 54.9 eV. Figures 4(a)–(f) shows SEM-FIB and cross-sectional micrographs of three tungsten samples.

ImageJ software [25] has been used to measure the average width of nano-tendrils shown in three SEM images. One hundred values were taken to determine the average width for each SEM image. Figure 5 shows that as the surface temperature increases from 1100 K to 1150 K, the nano-tendril width roughly increases two-folds from 46 nm to 101 nm, respectively.

The thickness of a HiPIMS grown fuzzy tungsten layer increased from 274 nm to 501 nm as the surface temperature rose by 125 K. This finding agrees with previous studies, which suggest that an increase in the surface temperature of tungsten enhances the growth rate of a fuzz on a plasma-exposed tungsten surface [26]. Kajita *et al* [24] showed that changes in $T_s$ have a substantial impact on the width of the nano-tendrils. Furthermore, the nano-bubbles increase in size as they move and merge due to thermal migration. Accordingly, the creation of vacancies is a crucial element that significantly affects the formation and expansion of these bubbles. As a result, elevated temperatures lead to larger helium bubbles, wider

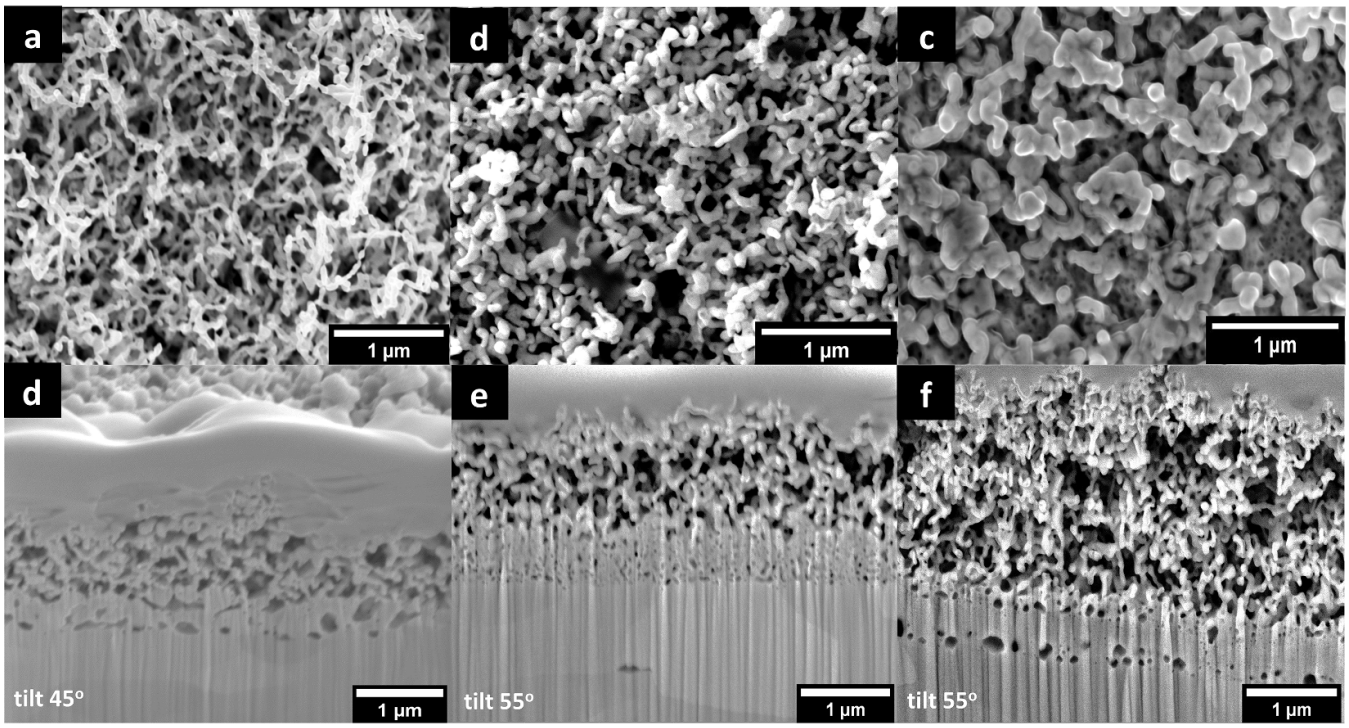


**Figure 3.** SEM-FIB and cross-sectional images of fuzzy W surfaces grown in a helium DC discharge with a helium ion fluence of $6.54 \times 10^{24}$ $m^{-2}$, ion bombarding energy of 54 eV and surface temperatures of (a), (d) 1025 K, (b, e) 1100 K and (c), (f) 1150 K.

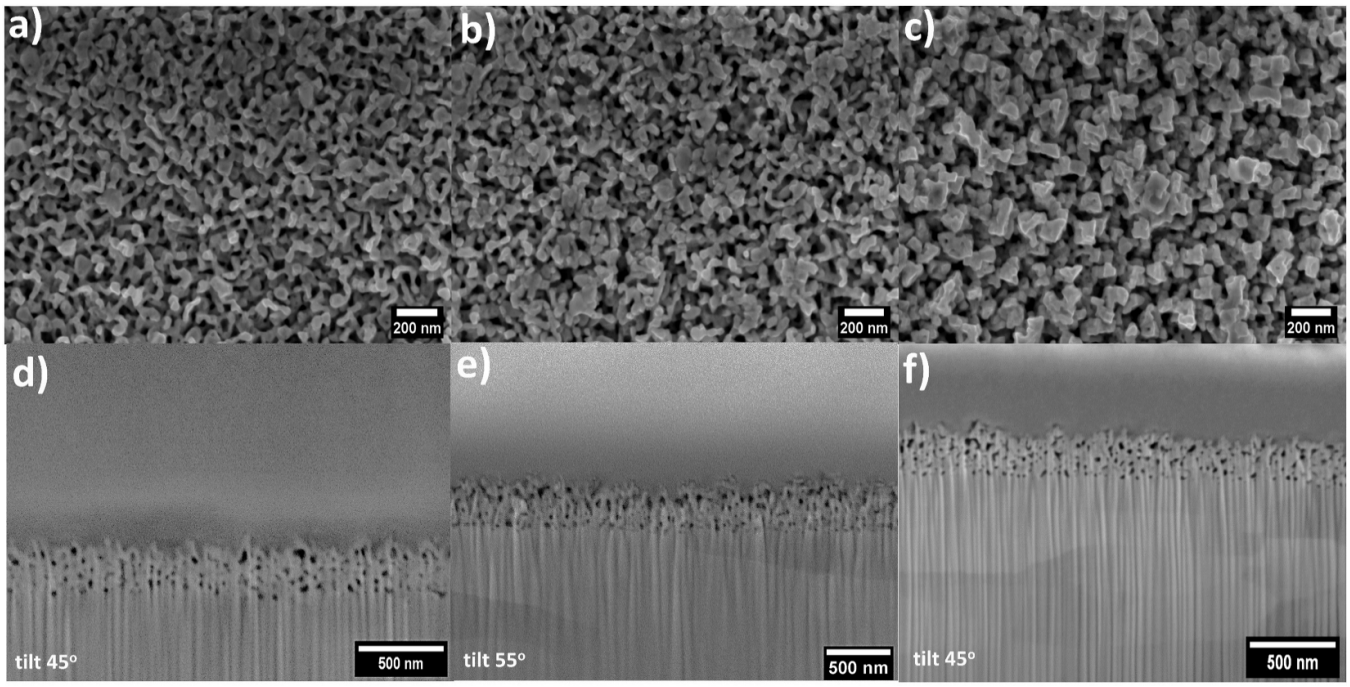


**Figure 4.** SEM-FIB and cross-sectional images of three fuzzy W surfaces grown in a helium HiPIMS discharge with an ion fluence of $5.02 \times 10^{24}$ $m^{-2}$, time averaged ion bombarding energy of 54.91 eV and surface temperatures (a), (d) 1025 K, (b), (e) 1100 K and (c), (f) 1150 K.

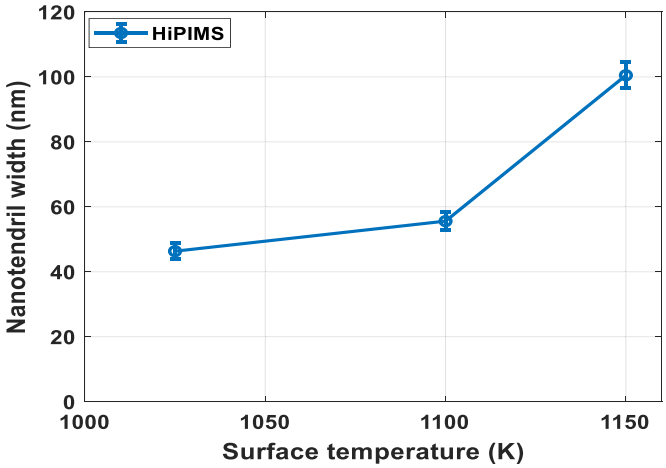


**Figure 5.** A plot of a HiPIMS grown nano-tendril width versus surface temperatures for a helium ion fluence of $5.02 \times 10^{24}$ $m^{-2}$ and time-averaged ion bombarding energy of 54.9 eV.

nanostructured tendrils and enhanced growth rate of fuzzy tungsten.

### 3.3. High resolution STEM images of HiPIMS-grown fuzzy W

The high-resolution STEM technique [27] was used to image the nano-tendril fuzzy tungsten irradiated by helium ions in HiPIMS discharge with an ion fluence of $5.02 \times 10^{24}$ $m^{-2}$, time averaged ion bombarding energy of 54.91 eV and surface temperatures of 1100 K.

STEM micrographs shown in figures 3(a)–(f), reveal the inner nanostructures of the fuzz layer grown on the tungsten substrate. In this case, the bottom of the nanostructure contains several small bubbles that may merge to create larger ones. However, these larger bubbles are not present at the top of the fuzz. Additionally, it has been observed that the bubbles found within the tendrils exhibit varying shapes and sizes, with no particular shape dominating or consistently appearing from one end of a tendril to the other.

Figures 6(g)–(h) suggest that the width (diameter) and length (vertical height) ranges of nano-tendrils across fuzzy tungsten layer are (2–50 nm), (3–158 nm) respectively, and helium nanobubbles range in size range of 5–120 nm are distributed throughout the sample, as shown in figure 6(i), creating porosity within the fuzz layer.

### 3.4. Comparison between a fuzz grown in HiPIMS and DCMS plasmas

In this study, we observed that the growth rates of the fuzzy tungsten layers grown in DC conventional magnetron sputtering, with a helium ion fluence of $6.54 \times 10^{24}$ $m^{-2}$, were approximately two-fold, compared to their values produced by high-power impulse magnetron sputtering plasma ($\Phi_{He} \sim 5.02 \times 10^{24}$ $m^{-2}$) at the same surface temperatures range (1025–1150 K), as shown in figure 7.

This result may be due to various causes firstly. A helium ion fluence in a DCMS grown fuzzy layer is slightly higher than that produced in a HiPIMS discharge, more helium bubbles would lead to the production of more protrusion and faster growth of fuzz layer [28]. Secondly, the growth of nano-tendrils is likely to be influenced by the deposition of sputtered Tungsten (W) atoms onto fuzzy tungsten during the helium plasma exposure. It was suggested that the deposited tungsten atoms integrate into the growing fuzzy tungsten layer [29]. McCarthy *et al* [17] concluded that when the ratio of W atoms to He ions reaching a tungsten surface is increased from 0.003 to 0.009 for the same helium ion fluence, it results in a doubling of the thickness of the fuzz layer grown in DCMS device. Kajita *et al* [20, 30] have demonstrated that, the growth rate of fuzzy tungsten was substantially enhanced by the metallic deposition, resulting in the development of noticeable large-scale fuzz. In addition, and due to the intrinsic properties of the magnetron sputtering device, the deposition rate plays an essential role in determining the thickness of the nanostructured tungsten layer. Consequently, the growth and deposition rates in HiPIMS discharge is normally lower than that in a conventional magnetron sputtering, which is caused by metal particles with low energy levels that return to the magnetron target through self-sputtering. Several hypotheses have been proposed to explain the reduced deposition and growth rate reported in HiPIMS discharge [21, 31]. The scientific community widely agrees on the phenomenon of ionized-sputtered material being drawn back to the magnetron target, and this occurrence is measured by the back-attraction probability, which significantly contributes to decreasing the quantity of sputtered particles that reach the substrate [32]. The decrease in the deposition rate (R) in HiPIMS is primarily attributed to the robust electric fields existing in the extended and presheath presheaths. The reduction in R notably relies on the material of the magnetron target [33]. Additionally, it is affected by various process parameters, including operating gas pressure, pulse frequency, pulse width, and the configuration of the magnetic field [32, 34, 35].

Moreover, the negative pulse width utilized in this study was relatively high (150 $\mu$s), which may have led to

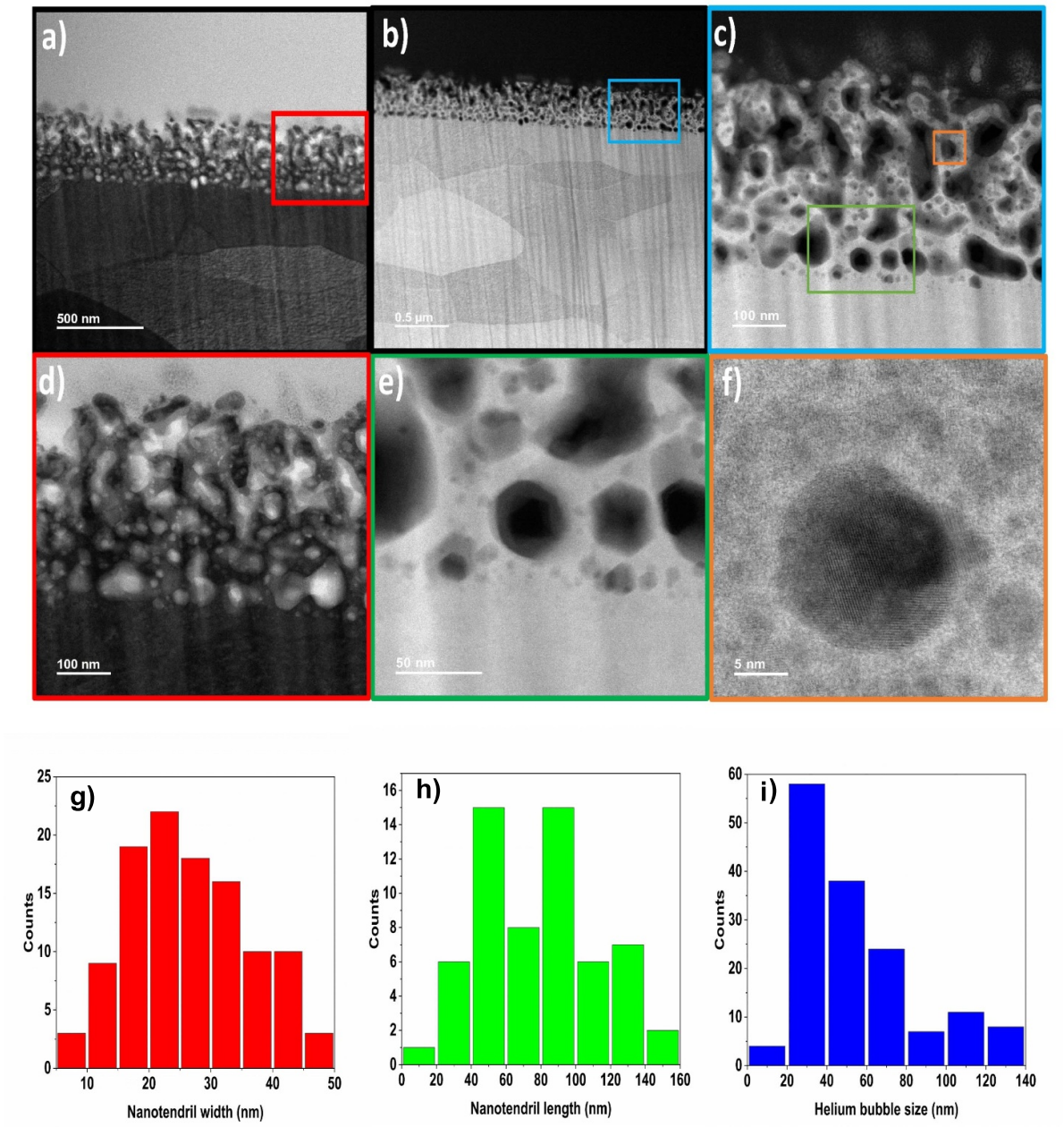


**Figure 6.** STEM micrographs of the fuzzy tungsten grown in HiPIMS at the surface temperature of 1100 K, helium ion fluence of $5.02 \times 10^{24}$ $m^{-2}$ and ion bombarding energy of 54.9 eV, (a) and (b) are low magnification BF and HAADF STEM images of the nano-tendrils respectively, (c) HAADF- STEM image is the magnified section of the nano-tendril shown in image (b), (d) BF- STEM image is the magnified section of the nana-tendril shown in image (a), (e) and (f) HAADF- STEM images are magnified sections of the nano-bubbles shown in image (c). Histograms (g)–(h) represent the width and length of tendrils across the fuzzy tungsten layer, and (i) histogram shows the size of helium bubbles in the fuzzy layer.

considerable gas rarefaction and ultimately decreased the number of ions that were available for the sputtering process.

Lastly, a higher HiPIMS frequency, in our experiment was 1.2 kHz, may cause a decrease in the thickness of the fuzz layer due to the dead time within the main negative pulse, which lies in the range of 500–1000 nm. During this time period, trivial amounts of sputtered metals occur which significantly increase with a rise in repetition frequency [36].

During the current experiments, we have not quantified the sputtering and deposition rates. Therefore, it is crucial to explore the relation between the deposition quantity and the rate of growth on a range of helium ion fluences in the future experiments. Nevertheless, due to the simultaneous occurrence of sample erosion, the mass loss method was not considered as an accurate process to determine the quantity of deposition.

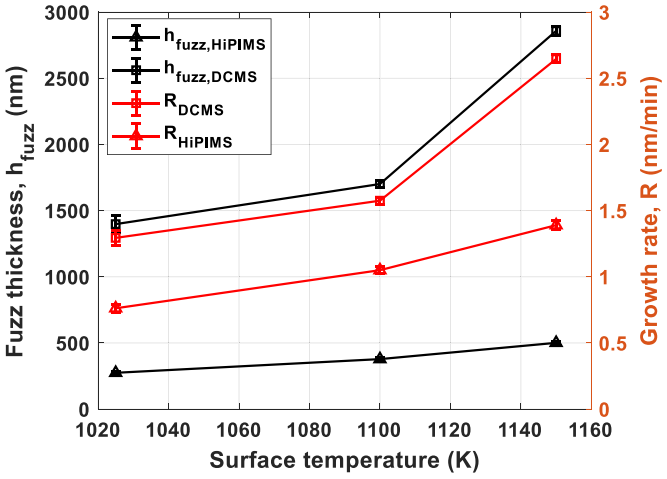


**Figure 7.** Plot of thickness and growth rate of fuzzy tungsten layers grown in a HiPIMS at $\Phi_{He} \sim 5.02 \times 10^{24}$ m$^{-2}$ and a DCMS at $\Phi_{He} \sim 6.54 \times 10^{24}$ m$^{-2}$ versus a surface temperature.

As far as sample roughness is concerned, results indicated that the roughness of the fuzz is directly related to its thickness, with rougher surfaces resulting from thicker samples. The mean roughness for samples irradiated with HiPIMS and DCMS at the same surface temperature of 1100 K were measured to be 14.87 ± 1.7 nm and 135 ± 12 nm, respectively. This provides evidence that the nanostructured tungsten grown in HiPIMS plasma is much smoother than that produced in a conventional magnetron sputtering.

## 4. Conclusions

In this study, a helium-high power impulse magnetron sputtering discharge (HiPIMS) was used to grow a nanostructured layer known as 'fuzz' on a bulk tungsten sample under divertor-like conditions. Herein, fuzzy tungsten was produced at a surface temperature range of 1025–1150 K, average helium ion fluence of $5.02 \times 10^{24}$ m$^{-2}$, and an average ion bombardment energy of 54.9 eV. The micrographic analysis has revealed that changes in $T_s$ resulted in a significant increase in the width of the nano-tendrils. In addition, we observed that the thickness of the fuzzy tungsten, measured by FIB-SEM cross-sectional micrographs, increased by 83% (from 274 to 501 nm) for only a 125 K rise in $T_s$.

The growth rate of fuzzy layer created in HiPIMS is compared to that grown in a DCMS for the same surface temperature range (752 °C–877 °C). Accordingly, the experimental results show that the growth rates of fuzzy tungsten layers were roughly twice the values in HiPIMS discharge. This finding could be attributed to many factors. Initially, the growth of nano-tendrils could be impacted by the deposition of sputtered W atoms onto fuzzy tungsten during the exposure to helium plasma. This suggests that a high porosity W surface would coalesce with deposited atoms, resulting in a more substantial increase in the fuzz thickness. Furthermore, in HiPIMS plasmas metal ions sputtered from the target with low energy can readily return to the target. An effect that is important in DCMS. HADDF/BF STEM images clearly illustrate that helium nano-bubbles with different sizes (5–120 nm) nm are distributed throughout the fuzzy tungsten exposed to HiPIMS plasma at the surface temperature of 1100 K, creating porosity within the fuzz layer.

## Data availability statement

All data that support the findings of this study are included within the article (and any supplementary files).

## Acknowledgments

The authors would like to thank Emre Yildirim (University of Manchester, UK) for his assistance in imaging tungsten surfaces and Felix Walk (University of Liverpool, UK) for setting up the HiPIMS unit. This study was partly funded by the University of Liverpool, UK.

## CRediT authorship contribution statement

Zeyad Ali: Investigation, data curation, data analysis, imaging, writing, and editing-original draft. Mounib Bahri: Data analysis, FIB, and STEM imaging. Matthew Bilton: Data analysis, SEM, and SEM-FIB imaging. James Bradley: Supervision, review, writing, editing, and funding acquisition.

## ORCID iDs

Zeyad Ali https://orcid.org/0009-0001-8830-3617
Mounib Bahri https://orcid.org/0000-0002-8336-9158
Matthew Bilton https://orcid.org/0000-0002-0475-2942
James W Bradley https://orcid.org/0000-0002-8833-0180

## References

[1] Iwakiri H, Yasunaga K, Morishita K and Yoshida N 2000 Microstructure evolution in tungsten during low-energy helium ion irradiation *J. Nucl. Mater.* **283** 1134–8
[2] Al-Ajlony A, Tripathi J and Hassanein A 2017 Low energy helium ion irradiation induced nanostructure formation on tungsten surface *J. Nucl. Mater.* **488** 1–8
[3] Qian W, Wei R, Zhang M, Chen P, Wang L, Liu X, Chen J, Ni W and Zheng P 2022 Fuzz formation on grain-refined bulk tungsten surfaces after low energy helium plasma exposure *Mater. Lett.* **308** 130921
[4] Jackson M *et al* 2023 The Erosion of selected tungsten coatings by ion beam and plasma sources compared to calculated predictions *Fusion Eng. Des.* **192** 113781
[5] Fiflis P, Curreli D and Ruzic D 2015 Direct time-resolved observation of tungsten nanostructured growth due to helium plasma exposure *Nucl. Fusion* **55** 033020
[6] Kajita S, Sakaguchi W, Ohno N, Yoshida N and Saeki T 2009 Formation process of tungsten nanostructure by the exposure to helium plasma under fusion relevant plasma conditions *Nucl. Fusion* **49** 095005
[7] Kajita S, Kawaguchi S, Ohno N and Yoshida N 2018 Enhanced growth of large-scale nanostructures with metallic ion precipitation in helium plasmas *Sci. Rep.* **8** 56

[8] Baldwin M and Doerner R 2010 Formation of helium induced nanostructure 'fuzz'on various tungsten grades *J. Nucl. Mater.* **404** 165–73
[9] Kajita S, Saeki T, Yoshida N, Ohno N and Iwamae A 2010 Nanostructured black metal: novel fabrication method by use of self-growing helium bubbles *Appl. Phys. Express* **3** 085204
[10] Wright G, Brunner D, Baldwin M J, Doerner R P, Labombard B, Lipschultz B, Terry J L and Whyte D G 2012 Tungsten nano-tendril growth in the Alcator C-Mod divertor *Nucl. Fusion* **52** 042003
[11] Matějíček J, Weinzettl V, Vilémová M, Morgan T W, De Temmerman G, Dimitrova M, Cavalier J, Adámek J, Seidl J and Jäger A 2017 ELM-induced arcing on tungsten fuzz in the COMPASS divertor region *J. Nucl. Mater.* **492** 204–12
[12] Tsitrone E *et al* 2022 Investigation of plasma wall interactions between tungsten plasma facing components and helium plasmas in the WEST tokamak *Nucl. Fusion* **62** 076028
[13] Wang K, Doerner R P, Baldwin M J and Parish C M 2018 Nucleation and growth of tungsten nanotendrils grown under divertor-like conditions *J. Nucl. Mater.* **509** 679–86
[14] Ohno N, Hirahata Y, Yamagiwa M, Kajita S, Takagi M, Yoshida N, Yoshihara R, Tokunaga T and Tokitani M 2013 Influence of crystal orientation on damages of tungsten exposed to helium plasma *J. Nucl. Mater.* **438** S879–82
[15] Khan A, De Temmerman G, Morgan T W and Ward M B 2016 Effect of rhenium addition on tungsten fuzz formation in helium plasmas *J. Nucl. Mater.* **474** 99–104
[16] Petty T, Khan A, Heil T and Bradley J 2016 Fuzzy tungsten in a magnetron sputtering device *J. Nucl. Mater.* **480** 374–85
[17] McCarthy P, Hwangbo D, Bilton M, Kajita S and Bradley J W 2020 Enhanced fuzzy tungsten growth in the presence of tungsten deposition *Nucl. Fusion* **60** 026012
[18] Petty T and Bradley J 2014 Tungsten nanostructure formation in a magnetron sputtering device *J. Nucl. Mater.* **453** 320–2
[19] Hori K, Kajita S, Zhang R, Tanaka H and Ohno N 2023 Growth origin of large-scale fiberform nanostructures in He–W co-deposition environment *Sci. Rep.* **13** 5450
[20] Kajita S, Kawaguchi S, Yoshida N, Ohno N and Tanaka H 2018 Morphologies of co-depositing W layer formed during He plasma irradiation *Nucl. Fusion* **58** 106002
[21] Anders A 2011 Discharge physics of high power impulse magnetron sputtering *Surf. Coat. Technol.* **205** S1–S9
[22] Lundin D, Minea T and Gudmundsson J T 2019 *High Power Impulse Magnetron Sputtering: Fundamentals, Technologies, Challenges and Applications* (Elsevier)
[23] Ryan P J, Bradley J W and Bowden M D 2019 Comparison of Langmuir probe and laser Thomson scattering for plasma density and electron temperature measurements in HiPIMS plasma *Phys. Plasmas* **26** 040702
[24] Kajita S, Yoshida N, Yoshihara R, Ohno N and Yamagiwa M 2011 TEM observation of the growth process of helium nanobubbles on tungsten: nanostructure formation mechanism *J. Nucl. Mater.* **418** 152–8
[25] Collins T J 2007 ImageJ for microscopy *Biotechniques* **43** S25–30
[26] Baldwin M and Doerner R 2008 Helium induced nanoscopic morphology on tungsten under fusion relevant plasma conditions *Nucl. Fusion* **48** 035001
[27] Pennycook S J and Nellist P D 2011 *Scanning Transmission Electron Microscopy: Imaging and Analysis* (Springer)
[28] Doerner R, Baldwin M, Simmonds M, Yu J, Buzi L and Schwarz-Selinger T 2017 Quantitatively measuring the influence of helium in plasma-exposed tungsten *Nucl. Mater. Energy* **12** 372–8
[29] Petty T, Baldwin M, Hasan M, Doerner R and Bradley J 2015 Tungsten 'fuzz'growth re-examined: the dependence on ion fluence in non-erosive and erosive helium plasma *Nucl. Fusion* **55** 093033
[30] Kajita S, Morgan T, Tanaka H, Hayashi Y, Yoshida N, Nagata D, Vernimmen J, Feng S, Zhang R and Ohno N 2021 Accelerated/reduced growth of tungsten fuzz by deposition of metals *J. Nucl. Mater.* **548** 152844
[31] Anders A 2010 Deposition rates of high power impulse magnetron sputtering: physics and economics *J. Vac. Sci. Technol.* A **28** 783–90
[32] Hajihoseini H, Čada M, Hubička Z, Ünaldi S, Raadu M A, Brenning N, Gudmundsson J T and Lundin D 2019 The effect of magnetic field strength and geometry on the deposition rate and ionized flux fraction in the HiPIMS discharge *Plasma* **2** 201–21
[33] Samuelsson M, Lundin D, Jensen J, Raadu M A, Gudmundsson J T and Helmersson U 2010 On the film density using high power impulse magnetron sputtering *Surf. Coat. Technol.* **205** 591–6
[34] Antonin O, Tiron V, Costin C, Popa G and Minea T 2014 On the HiPIMS benefits of multi-pulse operating mode *J. Phys. D: Appl. Phys.* **48** 015202
[35] Čapek J, Hála M, Zabeida O, Klemberg-Sapieha J and Martinu L 2013 Deposition rate enhancement in HiPIMS without compromising the ionized fraction of the deposition flux *J. Phys. D: Appl. Phys.* **46** 205205
[36] Bradley J, Mishra A and Kelly P 2015 The effect of changing the magnetic field strength on HiPIMS deposition rates *J. Phys. D: Appl. Phys.* **48** 215202